Effect of phosphorus on cleavage fracture in κ-carbide

N. I. Medvedeva,[1,2] R. A. Howell,[2] D. C. Van Aken,[2] and J. E. Medvedeva[2]
[1]*Institute of Solid State Chemistry, Yekaterinburg, Russia*
[2]*Missouri University of Science and Technology, Rolla, Missouri 65409, USA*
(Received 19 October 2009; revised manuscript received 23 December 2009; published 29 January 2010)

To understand the origin of cleavage fracture which dominates in Fe(Mn)-Al-C alloys at a high phosphorus concentration, we performed first-principles study of the phosphorus effect on ideal cleavage energy and critical stress in κ-carbide, Fe_3AlC, a precipitate in the austenitic alloys. We find that phosphorus has higher solubility in Fe_3AlC than in γ-Fe and sharply reduces the cleavage characteristics of κ-carbide. We show that strong anisotropy of the Fe-P bonds in $Fe_3(Al,P)C$ under tensile stress, leads to the appearance of large structural voids and may facilitate crack nucleation.

DOI: 10.1103/PhysRevB.81.012105 PACS number(s): 71.20.Be, 62.20.mm

Cubic ternary carbide Fe_3AlC (known as κ-carbide) precipitates in austenitic Fe-Al-C and Fe-Mn-Al-C alloys and plays an important role in age hardening properties.[1–8] The lightweight steels with high manganese content exhibit ultrahigh strength and excellent formability and are attractive for a wide range of applications.[7,9–12] The improved properties originate from the addition of aluminum that reduces the density of conventional Fe-Mn-C austenitic steels and produces an age hardenable steel. These alloys contain primary austenite (greater than 90%) and regularly distributed κ-carbide, which is coherent to the austenite matrix and precipitates when the aluminum and carbon contents exceed 5% and 0.3%, respectively.[5,7] Homogenous precipitation and dispersion of κ-carbide are the main mechanisms of hardening in these aluminum containing austenitic steels.

Impurities, even at a small concentration, may significantly affect the mechanical properties of the iron-based alloys. Among them is phosphorus which is known to reduce the toughness and ductility in high-strength iron steels due to the grain boundary embrittlement. The microscopic mechanism of phosphorus intergranular embrittlement is well studied in α-Fe, where phosphorus has a very low solubility in the bulk and a great propensity for segregation at grain boundaries.[13–17] Recent investigations of the cast Fe-Mn-Al-C alloys[8–10] also reveal a correlation of the toughness degradation with phosphorus content. However, not only intergranular failure but also transgranular cleavage fracture was observed in these alloys. The cleavage fracture is favored with increasing phosphorous content and the ductile to brittle transition occurs above the room temperature for P concentration $>0.04\%$. Similar fracture behavior has been found in wrought Fe-Mn-Al-C alloys, where alloy transitioned from ductile fracture to transgranular cleavage and finally to intergranular failure with increasing aging temperature.[2] A mixed mode of intergranular and transgranular cleavage was also observed[6] for the 0.006% phosphorus containing quenched Fe-Mn-Al-C alloys, whereas the transgranular cleavage is a dominant fracture mode in high phosphorus alloys (0.07%). Cleavage crack in steels is usually believed to initiate in the brittle precipitates such as carbides. Indeed, cleavage fracture was not observed in the austenitic alloys with suppressed degree of κ-carbide ordering, and so it was suggested[6,9,10] that crack nucleation originates in κ-carbide, however, the role of phosphorus in cleavage fracture was not understood.

In this study we focus on the microscopic origin of the phosphorus-induced cleavage fracture in κ-carbide. First, we calculated the solution enthalpy of phosphorus in various substitutional sites and predict its preferred location in bulk Fe_3AlC. Because the Fe-Mn-Al-C steels are primary austenite, it is important to know the phosphorus distribution between κ-carbide and austenite matrix. Therefore, we also estimated the solution enthalpy of phosphorus in γ-Fe and compared the results with those for Fe_3AlC, that allows us to predict the phosphorus spatial partitioning between these fcc phases.

To understand the role of phosphorus in transgranular brittle fracture, we calculated the cleavage parameters for Fe_3AlC with and without phosphorus. First-principles atomistic simulations of cleavage fracture are informative to establish the failure mechanism and they have been successfully used for studying the brittle fracture of metals, carbides, and intermetallics.[18–26] To simulate crack formation, the cleavage characteristics (the ideal cleavage energy and critical stress) are determined under the rigid cleaving of crystal. Essentially, the first-principles atomistic approach allows one to relate the cleavage process with the electronic properties and chemical bonding, thus providing the microscopic reasons for brittle fracture.

First-principles calculations were performed by using the projector augmented waves method as implemented in the Vienna *ab initio* simulation package[27,28] with the generalized gradient approximation for the exchange-correlation energy.[29] We carried out nonmagnetic (NM) and spin-polarized calculations, the local magnetic moments were estimated through the integration over the atomic spheres with the appropriate radii. We used a kinetic-energy cutoff of 350 eV and the k-point sampling that get the converged total energies within 0.01 eV/cell for each case. In particular, the $12\times12\times12$ k mesh was taken for pure Fe_3AlC and γ-Fe phases, while for supercells modeling the substituted phases, cleavage, and tensile properties we used the $6\times6\times6$, $12\times12\times6$, and $6\times6\times6$ k meshes, respectively.

The κ-carbide, Fe_3AlC, has the $E2_1$ crystal structure,[30] where aluminum occupies the (0,0,0) position, iron is in the $(\frac{1}{2},\frac{1}{2},0)$ position, and carbon is located at the center octahe-

dral site $(\frac{1}{2},\frac{1}{2},\frac{1}{2})$. Our calculations show the ground state of Fe_3AlC to be ferromagnetic (FM) with an equilibrium lattice parameter of 3.753 Å, while the nonmagnetic state has the total energy higher by 0.1 eV/cell and the lattice parameter of 3.733 Å. The obtained results are in a good agreement with the experimental data [3.78 Å (Ref. 31)] and previous theoretical results: 3.78,[32] 3.75,[33] and 3.76 Å.[34] The local magnetic moment of iron is about $1.0\mu_B$ that agrees with the calculated value of $1.12\mu_B$.[34] A comparison of the magnetic properties in Fe_3AlC with those in Fe_3Al,[33–36] where the magnetic moment is twice larger, demonstrates that it is carbon that sharply reduces the magnetization in the Fe-Al-C system.

γ-Fe has a complex magnetic phase diagram. Within the temperatures of thermodynamic stability (1184–1665 K) γ-Fe is paramagnetic, while the spin-spiral antiferromagnetic structure was found for the Fe precipitates in a Cu matrix.[37] Theoretical studies predict a competition between the ferromagnetic and antiferromagnetic (collinear and spin-density wave) structures, which differ only slightly in the total energy and volume.[38–40] For our calculations we choose the ferromagnetic high-spin (HS) state which has the largest lattice constant (3.65 Å) among the magnetic structures and, hence, provides a better mismatch between fcc Fe_3AlC and γ-Fe phases. Our goal is to estimate the solution enthalpy of nonmagnetic impurity, and we expect little sensitivity of the binding energy on the magnetic states, which differ in energy by less than 60 meV/atom.[38–40] We note that the ferromagnetic state was used to study the carbon diffusivity in γ-Fe.[41] For the cubic FM/HS state, we obtained the equilibrium lattice parameter of 3.64 Å and the local magnetic moment of $2.52\mu_B$, which both are in good agreement with previous *ab initio* calculations.[41,42]

First, we determined the energetically preferred location of phosphorus in bulk Fe_3AlC. We compared the solution enthalpy, ΔH_s, for the substituted phosphorus at $Fe(P_{Fe})$, $Al(P_{Al})$, or $C(P_C)$ site in the 40-atom $(2\times2\times2)$ supercells, where the lattice parameters and all atom positions were optimized. The same supercell size, cutoff, and k-points mesh were used for the undoped and substituted systems to make the comparison of energies more precise. The value of ΔH_s was estimated as the total-energy difference for supercell with phosphorus and ideal supercell taking into account the corresponding P substitution for Fe, Al, or C atom

$$\Delta H_s(P_{Fe}) = E(Fe_{23}PAl_8C_8) - E(Fe_{24}Al_8C_8) - [E(P) - E(Fe)],$$

$$\Delta H_s(P_{Al}) = E(Fe_{24}PAl_7C_8) - E(Fe_{24}Al_8C_8) - [E(P) - E(Al)],$$

$$\Delta H_s(P_C) = [E(Fe_{24}PAl_8C_7) - E(Fe_{24}Al_8C_8) - [E(P) - E(C)],$$

where for $E(A)$ we choose the energies of A=Fe, Al, C, or P metals in the bcc, fcc, graphite, and rhombic (black phosphorus) structures, respectively. It should be noted that the interstitial octa-site in Fe_3AlC is occupied by carbon atom. The solution enthalpy of substitutional and interstitial phosphorus in γ-Fe (which was modeled by using a 32-atom supercell) was calculated as

$$\Delta H_s = [E(Fe_{31}+P) - E(Fe_{32}) - E(P) + E(Fe)]$$

and

$$\Delta H_s = [E(Fe_{32}+P) - E(Fe_{32}) - E(P)],$$

respectively. For interstitial phosphorus we considered the octahedral position, which is more favorable for light impurities in γ-Fe than the tetra-site.[41,43] The calculated enthalpies for phosphorus in magnetic Fe_3AlC and γ-Fe are given in Table I along with the optimized lattice parameters and the distances between P and its nearest atoms. We found that the P substitution for Al does not change the lattice parameter, whereas P substituted in C position increases the lattice parameter in accord with their atomic-size difference. All substitutions reduce the magnetization to $0.84\mu_B$, (P_{Al}), $0.93\mu_B$ (P_C), and $0.78\mu_B$ (P_{Fe}).

TABLE I. Phosphorus substitution in Fe_3AlC: solution enthalpy ΔH_s, lattice parameter a, distances between P and the nearest Fe($R_{Fe\text{-}P}$) or C atoms ($R_{C\text{-}P}$).

	ΔH_s (eV)	a (Å)	$R_{Fe\text{-}P}$ (Å)	$R_{C\text{-}P}$ (Å)
Fe_3AlC: P_{Fe}	2.40	3.758	2.66	1.96
Fe_3AlC: P_{Al}	0.67	3.752	2.58	
Fe_3AlC: P_C	1.22	3.797	2.02	
γ-Fe: P_{Fe}	2.43	3.621	2.53	
γ-Fe: P_{int}	5.21	3.654	2.07	

Relaxation of the nearest atoms around phosphorus is inward for P at the Al site and outward for P substituting for the Fe or C atoms. For the Al, Fe, and C substitutions, the change in the distances between P and its nearest atoms is 2.8% ($R_{Fe\text{-}Al}$), 4.4% ($R_{C\text{-}P}$), and 7.6% ($R_{Fe\text{-}P}$), respectively, as compared to those in ideal Fe_3AlC. Thus, the smallest structural relaxation occurs for P substituted at Al site. Solution enthalpy is positive for all substitutions, and the lowest value corresponds to the phosphorus substitution for Al in Fe_3AlC. In this case the nearest twelve Fe atoms are shifted toward the P atom and form the strong covalent Fe-P bonds. Phosphorous substitutions for either C or Fe atoms are less stable (Table I) and these sites are unlikely for phosphorus.

In austenite, phosphorus prefers the substitutional site, while the solution enthalpy of the interstitial octa-position is larger by 2.8 eV (Table I). Similar result was obtained for phosphorus in bcc Fe, where the energy difference between the substitutional and octa-interstitial sites was estimated to be about 3 eV.[36,44] The lattice parameter decreases by 0.5% for the considered phosphorus concentration of 3 at. % and the nearest Fe atoms around substituted phosphorus in γ–Fe are shifted by −1.7% compared to the unrelaxed distance. The binding energies for P substituted for Fe are similar to those in κ-carbide (Table I), but for the preferred phosphorus sites (P_{Al} in Fe_3AlC) they differ significantly because the Fe-Fe bonds in γ Fe are much stronger than the Fe-P bonds.[44] Thus, we conclude that phosphorus in the Fe-Al-C

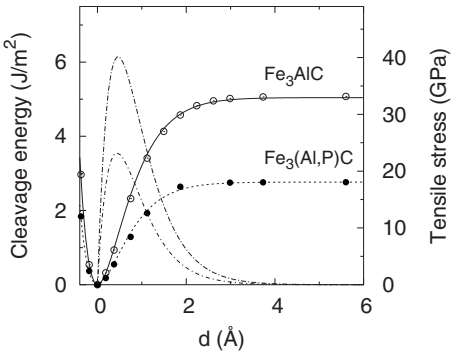

FIG. 1. Cleavage energies, $G_C(x)$, (solid line is the UBER fit) and cleavage stress $\sigma(x)$ (dotted line) versus cleavage separation in Fe_3AlC and $Fe_3(Al,P)C$.

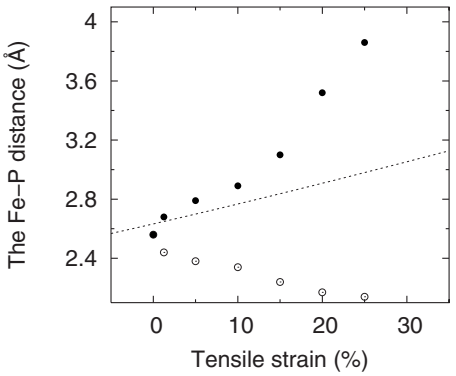

FIG. 2. The in-plane (open circles) and out-of-plane (filled circles) Fe-P distances as a function of tensile strain along ⟨001⟩ in $Fe_3(Al,P)C$. Dash line represents the out-of-plane Fe-P distance for the stretched lattice with no atomic relaxation.

alloys is most likely incorporates in κ-carbide, but not in austenite matrix. Below consider how phosphorus substituted for the most stable Al site in κ-carbide affects the cleavage fracture properties.

According to Griffith model, the intrinsic cleavage fracture takes place (or brittle cleavage propagates) when the mechanical energy of the loading stress exceeds the ideal cleavage energy G_C which is defined as the energy necessary to separate crystal into two semi-infinite parts. The dependence $G_C(x)$, where x is the separation distance between two crystal blocks, is fitted by the universal binding energy relation (UBER) $G_C(x)=G_C[1-(1+x)\exp(-x)]$, $x=u/\lambda$. The ideal cleavage stress may be calculated as $\sigma(x)=dG_C(x)/dx$, so that the parameter λ defines the distance which corresponds to the maximum stress σ_{max}. We modeled the (001) cleavage in Fe_3AlC (the {100} cleavage plane was inferred from the dendrite patterns produced by the fracture path[6]) by the repeated slab consisting of 12 layers and separated by a variable distance x. For the case of ideal brittle cleavage, no relaxation was allowed in the atomic positions after cleaving. Taking into account the structural relaxation after cleavage may overestimate sufficiently the critical cleavage stress, as it was shown recently.[26]

Cleavage energies $G_C(x)$ and stress $\sigma(x)$ versus cleavage separation between the (001) layers in nonmagnetic Fe_3AlC are shown in Fig. 1, where $x=0$ corresponds to the equilibrium interlayer distance in bulk. The results of UBER fit give the cleavage energy G_C and ideal critical stress σ_{max} of 5.04 J/m^2 and 40 GPa, respectively. Separation distance, λ, is 0.46 Å that corresponds to the ideal strain of 12%. We found that the ideal cleavage parameters are only slightly lower than, for example, those for FeAl (5.96 J/m^2 and 44 GPa).[23] To find how phosphorus affects the cleavage failure in Fe_3AlC, we assumed that crack is initiated in the plane with substituted impurity. Similar repeated slab construction from twelve (001) layers separated by a variable distance x was used to model the effect of P on the ideal cleavage characteristics. Phosphorus was placed at the Al site on one of the cleaving surfaces. Such arrangement corresponds to a 50% covering of the (001) surface by phosphorus and impurity concentration of 0.33 at. % in bulk. This concentration is certainly higher than that used in alloys, however, such a high-impurity concentration allows one to capture the local effect near impurity and better understand the observed trends. Our results (Fig. 1) show that phosphorus sharply decreases the ideal cleavage energy and the ideal cleavage stress, which we obtained for NM state to be 2.76 J/m^2 and 22 GPa, respectively, and they are 2.25 J/m^2 and 17 GPa for FM state. These values are half of those for ideal Fe_3AlC without P.

Magnetism is known to strongly affect the surface energy.[45] For both Fe_3AlC and $Fe_3(Al,P)C$, our spin-polarized calculations give a smaller G_C by about 20% as compared to the nonmagnetic states. The reduction is mainly due to the total-energy difference, whereas the lattice parameters for magnetic state increase by only 0.5%. We also find that the magnetic moment on iron atoms in the cleaved layers demonstrates the Friedel's oscillations with almost twice larger values for the outermost surface layers (namely, $1.8\mu_B$ and $2.0\mu_B$ for iron on the Fe-C and Fe-Al terminated surfaces, respectively, whereas the Fe magnetic moment in bulk is $1.0\mu_B$).

In order to understand the reason for the reduced cleavage characteristics, we modeled the tensile strain along the ⟨001⟩ direction by changing the c/a ratio in Fe_3AlC and $Fe_3(Al,P)C$. All atoms in supercell were allowed to relax in the stretched structures. We found that the relaxation plays a crucial role in the local geometry of the nearest and next-nearest atoms around phosphorus. First, phosphorus significantly enhances the anisotropy of the Fe-P bonds in Fe_3AlC under tensile stress. The in-plane and out-of-plane Fe-P distances decrease and increase, respectively, more sharply than it is expected for strained Fe_3AlC without P (dash line in Fig. 2). For the large tensile deformation (>15%), the in-plane Fe-P distances approach the value which corresponds to the molecular Fe-P systems (2.1 Å), while the out-of-plane Fe-P distances are significantly larger than the unrelaxed distance in the stretched crystal. Furthermore, the outward relaxation of the out-of-plane Fe atoms strongly weakens the Fe-Fe and Fe-Al bonds between the nearest and next nearest (001) layers [Figs. 3(a) and 3(b)]. As a result, these bonds accommodate a larger strain than the bonds between the other (001) layers. We suggest that manganese may enhance the embrittling effect of phosphorus due to formation of the strong in-plane Mn-P bonds,[14] whereas oversized impurities (e.g.,

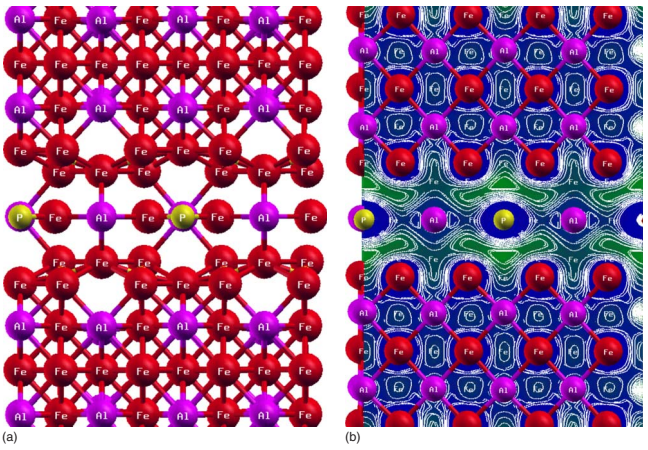

FIG. 3. (Color online). (a) The (101) projections of the relaxed crystal structure and (b) charge-density map for $Fe_3(Al,P)C$ under 25% tensile strain along ⟨001⟩.

Mo, Y, La) may weaken the in-plane bonding and improve the fracture properties.

Finally, we found that magnetism increases anisotropy of the Fe-P bonds resulting in larger voids. Magnetic moments of the nearest iron atoms sharply increase with tensile strain, and for the 15% strain they reach $1.8–1.9\mu_B$ that is similar to the Fe moments on the (001) surface of Fe_3AlC. For magnetic $Fe_3(Al,P)C$, the total energy required for this strain is less by 0.05 eV/atom (27%) than that for the nonmagnetic carbide—in accord with the fact that magnetic materials are usually softer under tension.

The structural voids in κ-carbide may serve as the preferred locations for crack nucleation, which occurs when plastic stress reaches the critical value. Uniformly arranged shear bands which formed due to the ordered distribution of κ-carbide and promote the enhanced ductility,[7] favor crack nucleation through the mechanism of dislocation coalescence. Indeed, crack in Fe-Mn-Al-C alloys was observed to follow the shear bands.[7,10] Additionally, as we showed, the applied tensile stress should play a large role in crack initiation and propagation.

In summary, using *ab initio* approach, we found the most stable phosphorus site in bulk Fe_3AlC and predicted the greater solubility of P in κ-carbide compared to austenite. Phosphorus substituted in bulk sharply reduces the brittle cleavage characteristics, the ideal cleavage energy and critical stress, and may facilitate crack nucleation and propagation. The calculations of $Fe_3(Al,P)C$ under tensile stress showed that the microscopic mechanism of phosphorus effect on cleavage fracture in κ-carbide originates from a strong anisotropy of Fe-P bonds under deformation that leads to the appearance of structural voids and strongly weakens the nearest interlayer Fe-Fe and Fe-Al bonds.

This work was supported in part by the AR Laboratory (Grant No. W911NF-07-D-0001) and the National Science Foundation (Grant No. CMMI-0726888). N.I.M acknowledges the support by the Russian Basic Research Foundation (Grant No. 09-03-00070a).

[1] P. J. James, J. Iron Steel Inst., London **207**, 54 (1969).
[2] G. E. Hale and A. J. Baker, *Alternate Alloying for Environment Resistance* (TMS-AIME Annual Meeting, Warrendale, PA, 1986).
[3] K. Sato *et al.*, Metall. Trans. A **21**, 5 (1990).
[4] K. H. Han and S. P. Hong, in *Alternate Alloying for Environmental Resistance*, edited by G. R. Smolik and S. K. Barnerji(The Metallurgical Society, 1987), pp. 91–106.
[5] Y. Kimura *et al.*, Mater. Sci. Eng., A **329-331**, 680 (2002).
[6] O. Acselrad *et al.*, Metall. Mater. Trans. A **35**, 3863 (2004).
[7] G. Frommeyer and U. Brux, J. Iron Steel Res. Int. **77**, 627 (2006).
[8] S. T. Chiou *et al.*, Mater. Sci. Eng., A **392**, 156 (2005).
[9] R. A. Howell *et al.*, AIST Trans. **6**, 168 (2009).
[10] R. A. Howell *et al.*, AFS Trans. **117**, 751 (2009).
[11] C. Scott *et al.*, Rev. Metall./Cah. Inf. Tech. **103**, 293 (2006).
[12] E. Mazancová *et al.*, Arch. Mater. Sci. **28**, 90 (2007).
[13] G. Druce *et al.*, Acta Metall. **34**, 641 (1986).
[14] R. Q. Wu *et al.*, J. Mater. Res. **72**, 403 (1992).
[15] L. P. Zhong *et al.*, Phys. Rev. B **55**, 11133 (1997).
[16] Y. Q. Fen and C. Y. Wang, Comput. Mater. Sci. **20**, 48 (2001).
[17] G. J. Ackland *et al.*, J. Phys.: Condens. Matter **16**, S2629 (2004).
[18] C. L. Fu and G. S. Painter, J. Mater. Res. **6**, 719 (1991).
[19] D. L. Price *et al.*, Phys. Rev. B **46**, 11368 (1992).
[20] M. H. Yoo, Mater. Sci. Eng., A **153**, 470 (1992).
[21] T. Hong *et al.*, Phys. Rev. B **45**, 8775 (1992).
[22] S. N. Sun *et al.*, Phys. Rev. B **54**, 3074 (1996).
[23] N. I. Medvedeva *et al.*, Phys. Rev. B **54**, 13506 (1996).
[24] I. G. Batirev *et al.*, Phys. Rev. Lett. **82**, 1510 (1999).
[25] Y. N. Gornostyrev *et al.*, Phys. Rev. B **62**, 7802 (2000).
[26] P. Lazar and R. Podloucky, Phys. Rev. B **78**, 104114 (2008).
[27] G. Kresse and J. Hafner, Phys. Rev. B **47**, 558 (1993).
[28] G. Kresse and J. Furthmuller, Phys. Rev. B **54**, 11169 (1996).
[29] J. P. Perdew and Y. Wang, Phys. Rev. B **45**, 13244 (1992).
[30] L. J. Huetter and H. H. Stadelmaier, Acta Metall. **6**, 367 (1958).
[31] P. Willars *et al.*, *Handbook of Ternary Alloy Phase Diagrams* (ASM, Metals Park, OH, 1995), Vol. 3.
[32] M. Ruda *et al.*, Scr. Mater. **46**, 349 (2002).
[33] P. Maugis *et al.*, Metall. Mater. Trans. A **37**, 3397 (2006).
[34] A. Kellou *et al.*, Phys. Status Solidi B **245**, 750 (2008).
[35] B. V. Reddy and S. C. Deevy, Mater. Sci. Eng., A **329-331**, 395 (2002).
[36] C. Domain and C. S. Becquart, Phys. Rev. B **71**, 214109 (2005).
[37] Y. Tsunoda, J. Phys.: Condens. Matter **1**, 10427 (1989).
[38] M. Uhl *et al.*, Phys. Rev. B **50**, 291 (1994).
[39] K. Knöpfle *et al.*, Phys. Rev. B **62**, 5564 (2000).
[40] E. G. Moroni *et al.*, J. Phys.: Condens. Matter **11**, L35 (1999).
[41] D. E. Jiang and E. A. Carter, Phys. Rev. B **67**, 214103 (2003).
[42] H. C. Herper *et al.*, Phys. Rev. B **60**, 3839 (1999).
[43] W. Pepperhoff and M. Acet, *Constitution and Magnetism of Iron and Its Alloys* (Springer-Verlag, Berlin, 2001).
[44] A. A. Vasiliev *et al.*, J. Nucl. Mater. **231**, 249 (1996).
[45] M. Alden *et al.*, Surf. Sci. **315**, 157 (1994).